VOL. 18, NO. 17, SEPTEMBER 2023 ISSN 1819-6608
ARPN Journal of Engineering and Applied Sciences

www.arpnjournals.com

STRUCTURAL, MAGNETIC AND OPTICAL PROPERTIES OF NICKEL DOPED IRON OXIDE NANOPARTICLES BASED ON LOGAS NATURAL SAND FOR ENVIRONMENTAL APPLICATION

Erwin Amiruddin[1,4], Amir Awaluddin[2], Martha Rianna[3], Miftahul Haqie Al Firdaus[4], Syavia Rofiqa[4], Sella Audina Putri[4] and Artika Dewi Sitangang[4]
[1]Department of Physics, Riau University, Pekanbaru, Indonesia
[2]Department of Chemistry, Riau University, Pekanbaru, Indonesia
[3]Department of Physics, North Sumatera University, Medan, Indonesia
[4]Magnetic Laboratory, Riau University, Pekanbaru, Indonesia
E-Mail:erwin_amiruddin@yahoo.com

ABSTRACT

The iron oxide nanoparticles have been prepared by mechanical milling method using Logas natural sand as a raw material. The products of ball milling were doped with Ni nanoparticles at different doping concentrations (0, 1, 2, 3, and 4 wt.%). The effect of doping concentration on the structural, magnetic, and optical properties was studied. The structural, magnetic, and optical properties of the prepared samples were studied using an X-ray diffractometer (XRD), vibration sample magnetometer (VSM), and UV-Vis spectroscopy, respectively. The X-ray diffraction pattern shows that the ball milling product is hematite (α-Fe_2O_3) nanoparticles and highly crystalline with a rhombohedral structure. It is very interesting to find that Ni doping nanoparticles cannot change the structure of iron oxide nanoparticles however, the average crystallite size decreases from 39.43 to 32.64 nm with increasing Ni doping concentration from 0 to 4 wt. %, respectively. The crystallite size based on the dominant peak (104) varies as Ni doping concentration increases. The magnetic properties of the samples show the ferromagnetic nature of the prepared nanoparticles. The saturation, remanence magnetization, and coercivity increase with increasing Ni concentration. The optical band gaps calculated through UV-Vis absorption measurements confirm that the decrease in crystallite size is accompanied by a decrease in the band gap value from 2.03 to 1.92 eV as the doping concentration increases from 0 to 4 wt. %.This study demonstrates the simple way of preparing Ni-doped iron oxide nanoparticles for environmental application.

Keywords: Logas natural sand, ball milling, Ni-doped, iron oxide nanoparticles.

Manuscript Received 26 July 2023; Revised 21 October 2023; Published 8 November 2023

INTRODUCTION

Nanomaterials especially iron oxide nanomaterials have attracted the attention of modern researchers due to their wide range of technical applications. Among various iron oxides of different forms (FeO, Fe_2O_3,and Fe_3O_4), the hematite iron oxides (α-Fe_2O_3) in the size of nanoscale are of great importance in technological and industrial applications [1]. Hematite exhibits high stability under ambient conditions and superparamagnetic behaviour [2,3] which has a wide range of applications including photocatalysis[4]. The applications of the iron oxide nanoparticles such as in environmental applications require certain properties which can be achieved by controlling the iron oxide nanoparticles preparation. Various techniques have been used to fabricate hematite nanoparticles of controllable morphology for various applications. There are several methods for preparing α- Fe_2O_3 nanoparticles including solar thermal,[5] laser pyrolysis,[6] thermal oxidation,[7] hydrothermal[8] methods. However, the simplest way to prepare hematite nanoparticles is the ball milling method[9]. It was observed that iron oxide nanoparticles show very different physical and chemical properties depending on their microstructure, such as size uniformity and crystallinity. Therefore, preparing magnetic nanoparticles thatcan maintain size uniformity and crystallinity is important. However, the development of a simple, reliable, and low-cost methodology to prepare magnetic iron oxide nanoparticles with controllable size and size distribution remains a challenging task for researchers.

For environmental applications, hematite (α-Fe_2O_3) nanoparticles are preferable due to their small band gap energy (2.1 eV)[10] and have ability to absorb visible light. However, these nanoparticles still have some limitations before applying them as photocatalysts. Several ways have been developed to overcome these limitations. One of them is to reduce the band gap of this type of iron oxide nanopraticles by doping hematite nanoparticles using different materials such as transition metal elements[11]. For example, previous researchers[12] used Sn, Nb, Pt, Zr, Ti, Zn, and Ni cations to modify the magnetic, structural as well and morphology of hematite nanoparticles using ball milling. Similar modifications have been reported for iron oxide using cobalt[13]. This modification may have the ability to control the structural, magnetic, andoptical properties of iron oxide nanoparticles and therefore can optimize them as catalysts. To modify the properties such as structural, magnetic, and optical properties of iron oxide nanoparticles, we report here the

effect of undoped and Ni-doped iron oxide nanoparticles based on Logas natural sand as a raw material on their structural, magnetic, and optical properties prepared using ball milling method.

EXPERIMENTAL METHOD

Raw Material and Chemical

For the preparation of iron oxide nanoparticles in this study, Logas natural sand was used as a raw material. The chemical used for doping the iron oxide nanoparticles is Ninanoparticleswith apurity of 99.99% was purchased at TokoPedia(www.tokopedia.com).

Preparation of Ni NI-Doped Iron Oxide Nanoparticles

Ni-doped iron oxide nanoparticles were prepared using the ball milling method. To separate between iron oxide and non-iron oxide particles, the sand sample was processed using an iron sand separator (ISS) and NdFeB magnet. The product was then milled using 4-stage ball milling. The milling was carried out for 50 hours of each stage. The iron oxide and non-iron oxide particles were separated again using a NdFeB magnet from the product of each stage. The product of the 4th stage of ball milling was divided into 5 parts with the same amount of weight. Ni nanoparticles were prepared for 0, 1, 2, 3, and 4 wt.%relative to the weight of the ball milling product. Each of these parts was milled together for20 hours.

Characterization Techniques

The prepared samples were characterized usingXRD, VSM, and UV-Visible Spectrophotometer. The XRD measurements were carried out using Cu-Kα radiation (1.5408 A˚). The scan range 2θ was from 10° to 100° at a scan speed of 5.0985^{o}/min and step width of 0.01°. The crystallite size was calculated using Scherrer equation (1), that is

$$D = \frac{k\lambda}{\beta \cos\theta} \text{……...……...……..(1)}$$

where λ is X-ray wavelength, k is constant β is the full width at half maximum (FWHM) and θ is Bragg's diffraction angle. The magnetic property of the samples was investigated using VSM with an applied magnetic field ranging from -20.000Oe to 20.000Oe. The UV-Vis absorption spectra of all the samples were obtained and the scanning range for the samples was 185–1100 nm.

RESULTS AND DISCUSSIONS

XRD Analysis

The XRD diffraction patterns of undoped and (1-4 wt.%) Ni-doped iron oxide nanoparticles are shown in Figure-1. The sharp and single diffraction peaks of the XRD pattern of the undoped sample shown in Figure-1(A) confirm the formation of crystalline α-Fe_2O_3. The various diffraction peaks of undoped iron oxide nanoparticles at 2θ 23.96°, 32.79°, 35.38°, 40.49°, 49.02°, 53.42°, 56.76°, 61.83° and 63.48° correspond to the refection from (012), (104), (110), (113), (024), (116), (122), (214) and (300) crystal planes, respectively. These peak positions correspond to the standard Bragg positions of hexagonal α-Fe_2O_3[14] which is in good agreement with the JCPDS No. 89-8103. The sharp and large intensity peaks observed in the XRD pattern indicate the formation of a highly crystalline hexagonal phase. It also can be noticed from Figure-1 that a small shift of the diffraction peaks occurs in most peak positions to slightly lower angles are observed for nickel-doped samples. Thisshiftofpeakpositionstoslightly loweranglesisshownintheinsetpatternsforthe expanded diffraction angle of 32.5^{o}- 33^{o}. This finding can be explained due to the milling and the formation of the nickel phase in the samples[15].

Figure-2 shows the XRD patterns of 4 wt.% Ni doped iron oxide nanoparticles and the insert is an XRD pattern for pure hematite (α-Fe_2O_3) as a comparison. The main peaks of 4 wt.% Ni doped iron oxide nanoparticles appear the same as those of undoped iron oxide nanoparticles andpure hematite (α-Fe_2O_3) nanoparticles inset in Figure-2. The average crystallite size and crystallite size for (104) reflection are estimated using Scherrer's formula[16] equation (1) of the Ni-doped iron oxide nanoparticles. The average crystallite sizes and crystallite size of (104) reflection of undoped and Ni-doped iron oxide nanoparticles decreases with increasing Ni concentration as shown in Figure-4. The decrease in the crystallite size is due to the enhancement in the density of nucleation centre in Ni-doped iron oxide nanoparticles[17]. The phase containing dopants (1-3 wt.% Ni) is observed in diffraction patterns especially(111) reflection as shown in Figure-1(B-E), which showed successful formation of ironoxide-nickel nanoparticles using ball milling. Moreover, in the Ni-doped sample with a concentration of 4 wt.%, the XRD patterns show an additional peak at a diffraction angle of 51.95^{o}whichcorresponds to the reflectionplane (200) as shown in Figure-2 which is characteristic of Ni (JCPDS no. 04-850)[18]. Therefore, the Ni dopant alters the crystallinity but not the crystal structure of iron oxide nanoparticles. The intensity of peaks (104) is gradually decreased with the Nidoping concentration as shown in Figure-3. Comparing the XRD patterns of undoped and Ni-doped nanoparticles of Figure-1, it can be seen that the higher the concentration of Ni added, the smaller the XRD spectrum intensity.

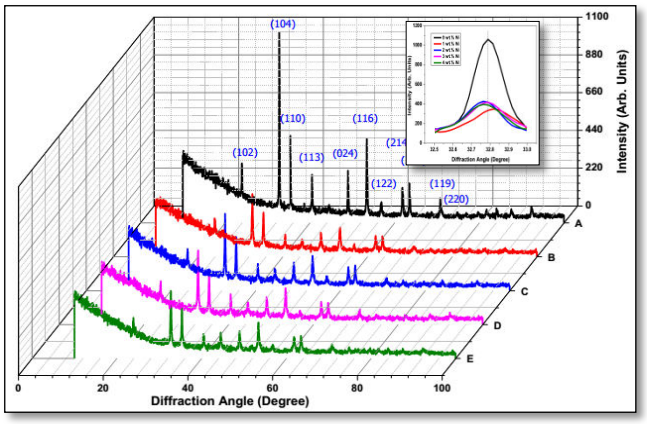

Figure-1.XRD patterns of Ni-doped (A) 0, (B) 1, (C) 2, (D) 3, and (E) 4 wt.% iron oxide nanoparticles. The inset patterns show the expanded diffraction angle of 32.5°-33° showing a shift of peak position to slightly lower angle.

By comparing the FWHM values, it can be found that the lower the diffraction peak, the higher the FWHM. By increasing Ni concentration, the FWHM of the samples first increases and then decreases and then slightly increases. This behaviour may be due to the change in diffraction intensity caused by the addition of Ni nanoparticles.

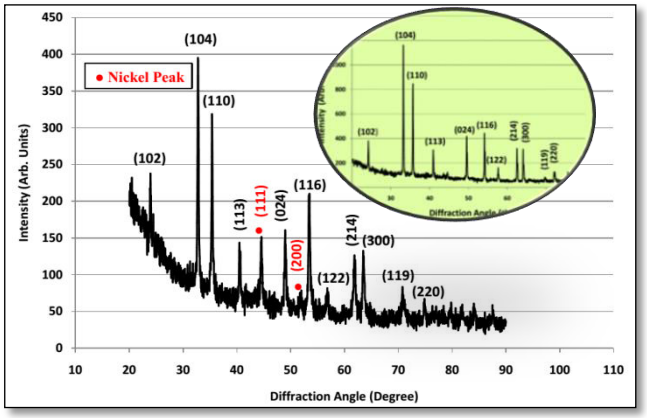

Figure-2. The XRD diffraction patterns of 4 wt.% Ni doped iron oxide nanoparticles. The inset pattern shows pure hematite (α-Fe_2O_3) nanoparticles showing high peak intensity.

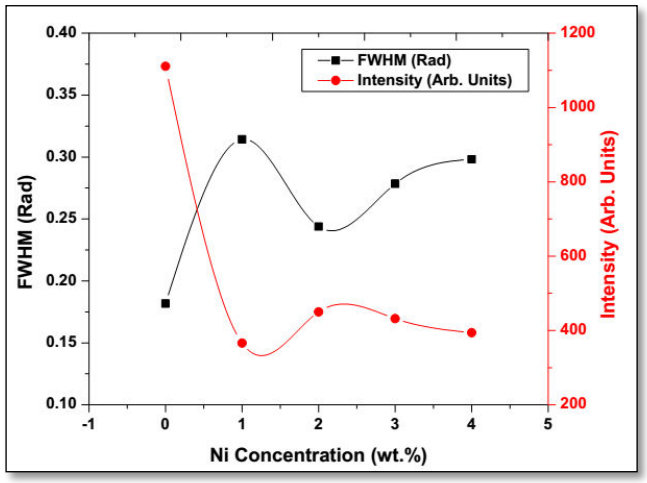

Figure-3. Variation of FWHM and intensity of peak (104) as a function of Niconcentration (wt.%) of iron oxide nanoparticles.

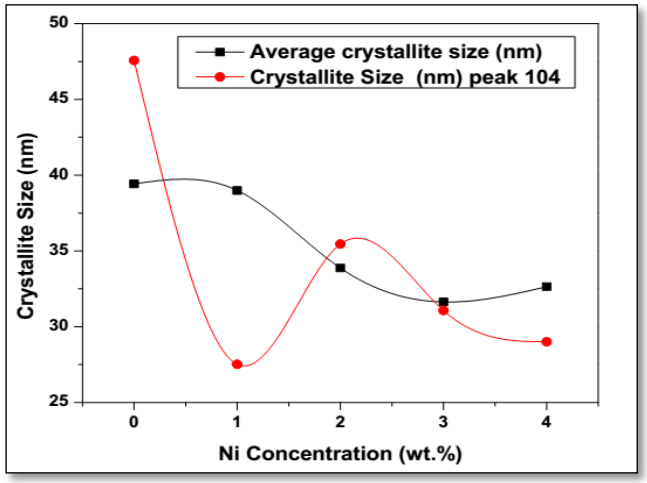

Figure-4. Variation of crystallite size (a) average and (b) peak (104) as a function of Niconcentration (wt.%) of iron oxide nanoparticles.

Magnetic Properties

The magnetic properties of undoped and Ni-doped iron oxide nanoparticles were studied using a vibration sample magnetometer (VSM) with an applied magnetic field ranging from -20,000Oe to +20,000Oe. Figure-5 shows the hysteresis loops of undoped iron oxide nanoparticles. It is seen that the hysteresis loop exhibits weak ferromagnetic behaviour which agrees with previous observations in earlier works [19]. Figure-6 shows the hysteresis loops of Ni-doped iron oxide nanoparticles with different Ni concentrations (wt.%), which exhibit weak ferromagnetic behaviour. A similar typeof weak ferromagneticphenomenon is also observed in cobalt iron oxide nanoparticles reported by previous work[19]. From the hysteresis loops, thesaturation magnetization (M_s), remanent magnetization (M_r), and coercivity (H_c) were calculated and theresults are presented in Figure-7. The

saturation magnetization and remanent magnetization of undoped iron oxide nanoparticles were observed at around 0.658 emu/g and 0.091 emu/g, respectively. The undoped iron oxide nanoparticles have a coercivity of about 120,23 Oe which is lower than that reported in previous literature[21]. Ms, Mr, and Hc values of the samples increasewhen the concentration of Ni is increased. In comparison, the saturation magnetization value of undoped iron oxide nanoparticles is slightly smaller than that of the pure hematite nanoparticles reported by previous researchers [22]. This is due to several factors such as size, crystalline and crystal defect[23], and the pureness of prepared iron oxide nanoparticles. The smaller coercivity for Ni-doped samples compared to that of other researchers[24] can be attributed to the difference in morphological properties and reduced magneto-crystalline anisotropy.

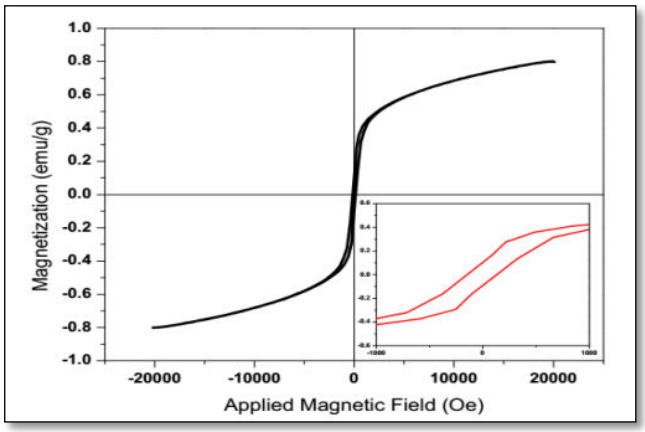

Figure-5. Hysteresis curves ofundoped iron oxide nano particles. The inset: magnification of the low-field region.

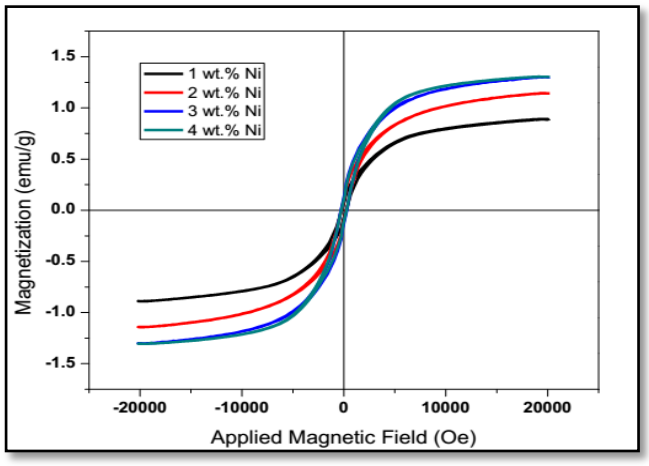

Figure-6. Hysteresis loops of Ni-doped iron oxide nano particles with different Ni concentrations (wt.%).

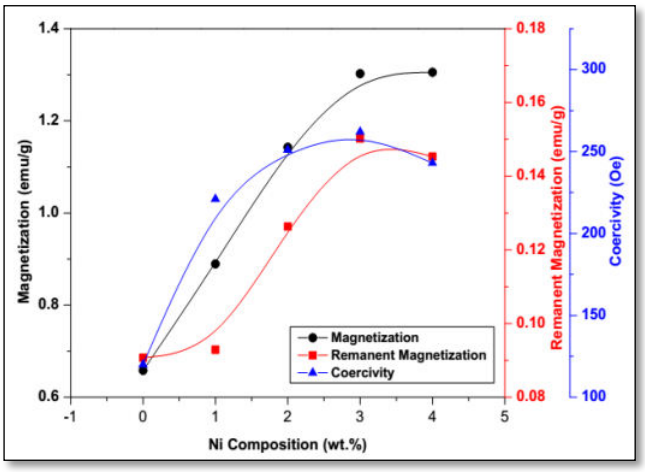

Figure-7. Saturation, remanent magnetization, and coercivity of iron oxide nanoparticles as a function ofNi concentration (wt.%).

Optical Properties

UV-visible optical absorption spectra of undoped and Ni-doped iron oxide nanoparticles measured in the range of 180-1100 nm wavelengths are shown in Figure-8.One absorption edge is observed between 200-300 nm for the samples. The absorption edges disappear as the wavelength increases. The intensity of the absorption peak increases with the increasing Ni concentration, as reported in the previous work[25].Strong absorption at wavelength 218, 233, 245, 264, and 233 nm is observediniron oxide nanoparticles for 0, 1, 2, 3, and 4 wt.% Ni doping, respectively. The strong absorption is found to shift towards higher wavelengths which are associatedwith lower energies as Ni concentration increases. According to previous researchers[26], this absorbance characteristic of nanoparticles depends on particle size, band gap, structure, and surface roughness.

The band gap values for absorption peaks of iron oxide nanoparticles are calculated from Tauc's relation[27]

$$\alpha h\nu = A\sqrt{E_g - h\nu} \quad \text{..... (2)}$$

where h is Planck constant, ν is frequency, α is the absorption coefficient n - either 1/2 for a direct transition or 2 for an indirect transition and A is the absorbance. Nanoparticles of α-Fe_2O_3have a direct band gap (n = 2)[28]. The band gap (Eg) of the samples is calculated from the intercept of the linear part of the curve in the plot of $(\alpha h\nu)^2$ on the y-axis versus photon energy (hν) on the x-axisas shown in Figure-10. The corresponding band gap and absorbance are shown in Figure-9. The band gap of undoped iron oxide nanoparticles is found to be 2.03 eV, which is smaller than that reported value of 2.1 eV in α-Fe_2O_3nanoparticles[10] and it decreases with increasing Ni doping concentration. The calculated band gap of Ni-doped iron oxide nanoparticles is in agreement with previous researchers[29]. Ni doping can narrow the optical

band gap value of iron oxide nanoparticles. The decreased band gap could be due to the increase in densityof the localized state in theconduction band[30]. The crystallite size reduces the band gap of nanoparticles, which is in good agreement with previous researchers[31]. This is because, with a decrease in particle size and average crystallite size, the band gap of the samples decreases.

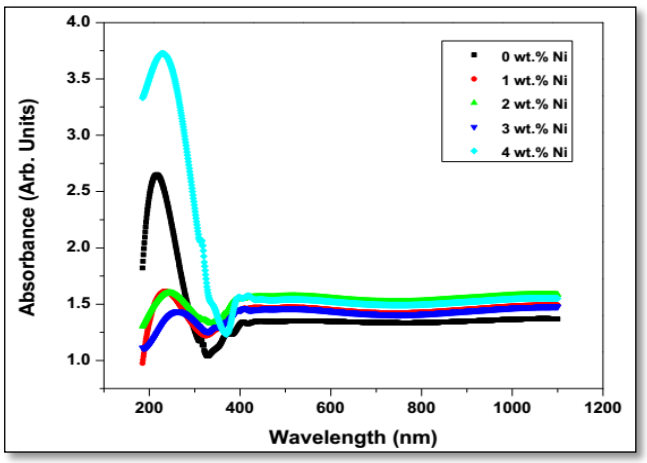

Figure-8. UV-visible spectra of undoped and Ni-doped iron oxide nanoparticles as a function of nickel concentration (wt.%).

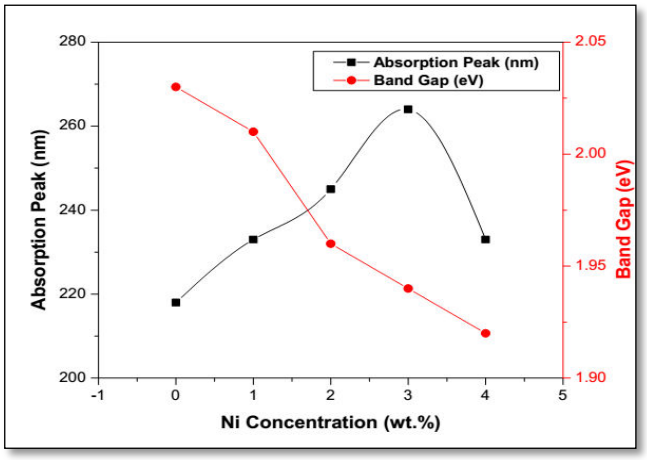

Figure-9. Absorption peaks and band gap of undoped and Ni-doped iron oxide nanoparticles as a function of nickel concentration (wt.%).

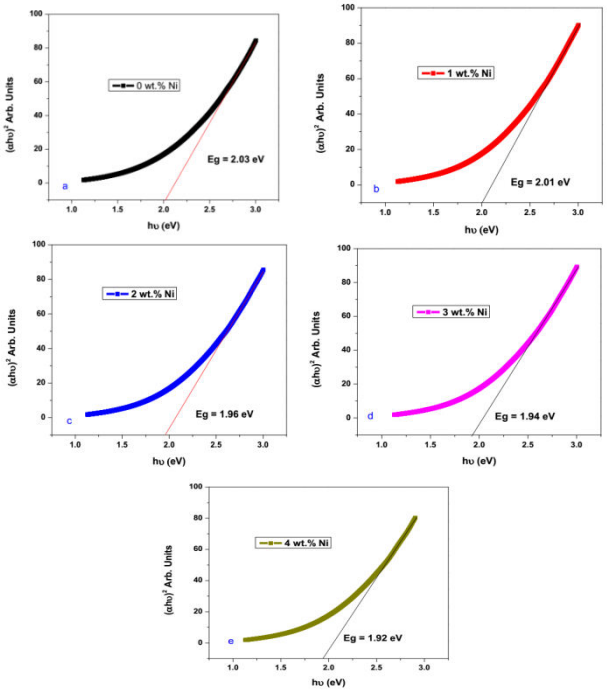

Figure-10. The optical band gap energy for (a) undoped and (b) 1 wt.%, (c) 2 wt.% (d) 3 wt.%, and (e) 4 wt.% Ni doped ironoxide nanoparticles.

CONCLUSIONS

In summary, undoped and Ni (1-4 wt.%) dopediron oxide nanoparticles based on Logas natural sand as a raw material were successfully prepared by a simple mechanical milling method. Structural studies revealed that particles are crystallized in the single-phase rhombohedral crystal structure of α-Fe_2O_3. The average crystallite size and crystallite size of (104) peak decreases with increasing Ni concentration. When the amount of Ni was added in iron oxide nanoparticles from 1 to 4 wt.%, a newpeak (111) was detected by XRD. However, an additional Ni peak (200) is observed for 4 wt. % Ni-doped iron oxide nanoparticles. The intensity of this (111) peak increases with increasing amount of Ni concentration. The existence of diffraction peaks related to the Ni and iron oxide nanoparticles showed a successful mechanical milling method to form iron oxide-Ni nanoparticles. The magnetic studies confirmthe ferromagnetic nature of the samples. The saturation, remanent magnetization, and coercivity of the samples increase with increasing Ni concentration. The optical band gap decreases with increasing Ni concentration. Optical absorption studies indicated higher wavelengths which are associatedwith lower energies as Ni concentration increases. The results indicated that the obtained iron oxide nanoparticles prepared by simple mechanical milling method as potential materials for environmental applications.

ACKNOWLEDGMENT

This work was financially supported by the Directorate General of Higher Education, Indonesian

Ministry of Education, Culture, Research, and Technology 2023. The authors are grateful to Indonesian Sciences Institute (LIPI), for conducting the VSM and SEM measurements, the Physics department UNP Padang for XRD and Uv-Vis measurements, and magnetic research members in Magnetic Laboratory FMIPA UNRI, for their assistance during sample collection and preparation.

REFERENCES

[1] K. L. Huo, W. Li, L. Lu, H. Cui, S. Xi, J. Wang, B. Zhao, Y. Shen, and Z. Lu. 2000. Preparation, structure, and properties of three-dimensional ordered α-Fe_2O_3nano-particulate film. Chem. Mater. 12(3): 790.

[2] Xu, P.; Zeng, G. M.; Huang, D. L.; Feng, C. L.; Hu, S.; Zhao, M. H.; Lai, C.; Wei, Z.; Huang, C.; Xie, G. X.; Liu, Z. F. 2012. Use of iron oxide nanomaterials in wastewater treatment: A review. Sci. Total Environ. 424: 1-10.

[3] Dumitrache F., Morjan I., Fleaca C., Badoi A., Manda G., Pop S., Marta D. S., Huminic G., Huminic A., Vekas L., Daia C., Marinica O., Luculescu C., Niculescu A. M. 2015. Highly magnetic Fe_2O_3 nanoparticles synthesized by laser pyrolysis are used for biological and heattransfer applications. Appl. Surf Sci. 336: 297-303.

[4] Moteb M. Alqahtani, Atif M. Ali, Farid A. Harraz, M. Faisal, Adel A. Ismail, Mahmoud A. Sayed, M.S. Al-Assiri. 2018. Highly Sensitive Ethanol Chemical Sensor Based on Novel Ag-Doped Mesoporous α–Fe2O3 Prepared by Modified Sol-Gel Process. Nanoscale Res. Lett. 13(157): 2-13.

[5] Zhu D., Zhang J., Song J., Wang H., Yu Z., Shen Y., Xie A. 2013. Efficient one-pot synthesis of hierarchical flower-like α- Fe_2O_3 hollow spheres with excellent adsorption performance for water treatment. Appl. Surf Sci. 284: 855-61.

[6] Dumitrache F., Morjan I., Fleaca C., Badoi A., Manda G., Pop S.,Marta D. S., Huminic G., Huminic A., Vekas L., Daia C., Marinica O., Luculescu C., Niculescu A. M. 2015. Highly magnetic Fe2O3nanoparticles synthesized by laser pyrolysis used for biological and heat transfer applications. Appl. Surf Sci. 336: 297-303.

[7] Su X., Yu C., Qiang C. 2011. Synthesis of α- Fe_2O_3 nano-belts and nanoflakes by thermal oxidation andstudy to their magnetic properties. Appl Surf Sci. 257: 9014-8.

[8] Tadica M., Panjan M., Damnjanovicc V., Milosevic I. 2014. Magnetic properties of hematite (α- Fe_2O_3) nanoparticles prepared by hydrothermal synthesis method. Appl Surf Sci. 320:183-7.

[9] Erwin Amiruddin, Amir Awaluddin, InnikeHariani, RibkaSihombing and RiskaAngraini. 2020. The Influence of Milling Ball Size on the Structural, Morphological and Catalytic Properties of Magnetite (Fe_3O_4)Nanoparticles toward MethyleneBlue Degradation. Journal of Physics: Conference Series 1655: 012006

[10] L. Li, Y. Yu, F. Meng, Y. Tan, J. R. Hamers, and S. Jin. 2012. Facile Solution Synthesis of α-$FeF_3 \cdot 3H_2O$ Nanowires and Their Conversion to α- Fe_2O_3 Nanowires for Photo-electrochemical Application. Nano Lett. 12: 724.

[11] CaiaL., Hua Z., Brantonb P. 2014. The effect of doping transition metal oxides on copper manganese oxides for the catalytic oxidation of CO Chinese J Catal. 35: 159-167.

[12] Malviya K. D., Dotan H., Shienkevich D., Tsyganok A., Mor H. and Rothschild A. 2016. Systematic comparison of different dopantsin thin films hematite (α- Fe_2O_3) photo anode for solar water splitting J. Mater. Chem. A. 4: 3091-3099.

[13] Erwin Amiruddin, Salomo Sinuraya, Amir Awaluddin, Rahmondia Nanda Setiadi, Muhammad Rizki, Novalia Magdalena Purba and Indah Tamara Sitorus. 2023. Magnetic and optical properties of cobalt-doped hematite nanoparticles of Logas natural sand for environmental application. ARPN Journal of Engineering and Applied Sciences. 18(4): 280-285

[14] K. Supattarasakda, K. Petcharoen, T. Permpool, A. Sirivat, W. Lerdwijitjarud. 2013. Control of hematitenanoparticle size and shape by the chemicalprecipitation method. Nanoparticles Technol. 249: 353-359.

[15] O. M. Lemine, Ghiloufi, M. Bououdina, L. Khezami, M. M'hamed and A. Taha. 2014. Nanocrystalline Ni doped α-Fe_2O_3 for Adsorption of Metals from Aqueous Solution. Journal of Alloys and Compounds. 588: 592-595.

[16] B. D. Cullity, S. R. Stock. 1978. Elements of X-ray Diffraction in Diffraction III: Real Samples, 3rdedn. 170 (Addison-Wesley, Boston, Chap. 5)

[17] Abdelmajid Lassoued, Mohamed Saber Lassoued, Santiago García‑Granda, Brahim Dkhil, Salah Ammar, Abdellatif Gadri. 2018. Synthesis and characterization of Ni-doped a-Fe_2O_3 nanoparticles through co-precipitation method with enhanced photocatalytic activities. J. Mater. Sci. Mater. Electron. 29: 5726-5737.

[18] A. Lassoued, M. S. Lassoued, S. García-Granda et al., Amrut S. Lanje, Satish J. Sharma and Ramchandra B. Pode. 2010. Magnetic and Electrical Properties of NickelNanoparticles prepared by Hydrazine Reduction Method. Scholars Research Library, Archives of Physics Research. 1(1): 49-56.

[19] Erwin Amiruddin, Salomo Sinuraya, Rahmondia N. Septiadi, Yanuar Hamzah, Amir Awaluddin, Loly A. Hardani, Fitri A. Lestari, Yessi Magdalena and Devi T. Gurning. 2022. A Systematic Study of the Structural and MagneticProperties of Nickel Doped α-Fe_2O_3 nanoparticles Prepared from Logas Natural Sand. ARPN Journal of Engineering and Applied Sciences. 17(14): 1408-1413.

[20] Erwin Amiruddin, Salomo Sinuraya, Amir Awaluddin, Rahmondia Nanda Setiadi, Muhammad Rizki, Novalia Magdalena Purba, and Indah Tamara Sitorus. 2023. Magnetic and Optical Properties of Cobalt-Doped Hematite Nanoparticles of Logas Natural Sand for Environmental Application. ARPN Journal of Engineering and Applied Sciences.18(4):280-285.

[21] Imen Grabsi, Faiza Bouaïcha, Aicha Ziouche, Nassima Bouaziz, Mourad Zaabat, Fikret Yildiz. 2022. Efect of Cobalt and Nickel Doping on Structural and Magnetic Properties of Iron Oxide Nanoparticles. Journal of Inorganic and Organo metallic Polymers and Materials. 32: 1287-1294.

[22] Akbar Ali Qureshi, Sofia Javed, Hafiz Muhammad Asif Javed, Muhammad Jamshaid, Usman Ali and Muhammad Aftab Akram. 2022. Systematic Investigation of Structural, Morphological, Thermal, Optoelectronic, and Magnetic Properties of High-PurityHematite/MagnetiteNanoparticles for Optoelectronics. Nanomaterials.12: 1635.

[23] X. L. Xie, H. Q. Yang, F. H. Zhang, L. Li, J. H. Ma, H. Jiao, J. Y. Zhang, 2009. Nanocrystalline α-Fe_2O_3: A Superparamagnetic Material forw-LED Application and Waste Water Treatment J. Alloys Compd. 477: 90-99.

[24] Arvind Yogi, Dinesh Varshney. 2013. Magnetic and structural properties of pure and Cr-doped haematite: α-Fe_2-xCr_xO_3 (0≤x≤1). Journal of Advanced Ceramics. 2(4): 360-369.

[25] Erwin Amiruddin, Salomo Sinuraya, Amir Awaluddin, Martha Rianna, Heri Hadianto, Muhammad Rizki, Novia Magdalena Purba and Indah Tamara Sitorus. 2023. Chromium Doped Iron Oxide Nanoparticles and Physical Properties Prepared from Logas Natural Sand and Their Application in Photo-Fenton Degradation of Methylene Blue Dye. ARPN Journal of Engineering and Applied Sciences. 18(10):

[26] Ahmed A. S., Shafeeq M. M., Singla M. L., Tabassum S., Naqvi A. H., Azam A. 2010. Band gap narrowing and fluorescence properties of nickel doped SnO_2 nanoparticles. J Lumin. 131: 1-6.

[27] Tauc J. 1974. Amorphous and Liquid Semiconductors, Plenum Press, New York. 171.

[28] Mohammadikish, M. 2014. Hydrothermal synthesis, characterization and optical properties of ellipsoid shape α-Fe_2O_3 nanocrystals. Ceram. Int. 40: 1351-1358.

[29] Nina Popov, Stjepko Krehula, Mira Risti´c, Ern″ o Kuzmann, Zolt´anHomonnay, Marko Bo˘skovi´c, Dalibor Stankovi´c, Shiro Kubuki, Svetozar Musi´c. 2021. Influence of Cr doping on the structural, magnetic, optical and photocatalytic properties of α-Fe_2O_3nanorods. Journal of Physics and Chemistry of Solids. 148(109699): 1-12.

[30] Prakash Chand, Anurag Gaur, Ashavani Kumar. 2014. Effect of Cr and Fe Doping on the Structural and Optical Properties of ZnO Nanostructures. World Academy of Science, Engineering and Technology International Journal of Chemical and Molecular Engineering. 8(12): 1321-1324.

[31] Lassoued A., Dkhil B., Gadri A. and Ammar S. 2017. Control of the shape and size of iron oxide (α-Fe_2O_3) nanoparticles synthesized through the chemical precipitation method Results Phys. 73007-15.